Calibration and Stability of Oxygen Sensors on Autonomous Floats

Eric A. D'Asaro[1] and Craig McNeil[2]

[1]*Applied Physics Laboratory and School of Oceanography, University of Washington*

Corresponding author:

1013 NE 40th Street, Seattle, WA, 98105

206 685 2982

dasaro@apl.washington.edu

[2]*Applied Physics Laboratory, University of Washington*

February 6, 2013

Abstract

The calibration accuracy and stability of three Aanderaa 3835 optodes and three Seabird SBE-43 oxygen sensors were evaluated over four years using *in situ* and laboratory calibrations. The sensors were mostly in storage, being in the ocean for typically only a few weeks per year and operated for only a few days per year. Both sensors measure partial pressure of oxygen, or equivalently saturation at standard pressure; results are expressed in this variable. It is assumed that sensor drift occurs in the oxygen sensitivity of the sensors, not the temperature compensation; this is well justified for the SBE-43 based on multiple calibrations. Neither sensor had significant long-term drift in output when sampling anoxic water. Sensor output at 100% saturation differed from the factory calibrations by up to ±6% (averaging –2.3%±3%) for the SBE-43 and up to –12.6% for the optodes. The optode output at 100% saturation is well described by a single decaying exponential with a decay constant of ~2 yr and an amplitude of 28%. The mechanism of this drift is unknown, but is not primarily due to sensor operation. It may be different from that experienced by sensors continuously deployed in the ocean. Thus, although the optodes in this study did not have a stable calibration, their drift was stable and, once calibrated, allowed optode and SBE-43 pairs mounted on the same autonomous floats to be calibrated to an accuracy of ±0.4% over a 4-yr period.

1. Introduction

Measurement of oxygen on moorings, floats, gliders, and other autonomous oceanographic platforms is becoming common. For example, several hundred ARGO floats have been equipped with oxygen sensors (Körtzinger et al. 2005), each measuring many dozen profiles per year. Detailed observations of air–sea oxygen fluxes (D'Asaro and McNeil 2007; Kihm and Körtzinger 2010), biological productivity (Riser and Johnson 2008, Alkire et al. 2012), and oxygen minimum zones (Prakesh et al. 2012) have been made using such systems. However, the absolute calibration of oxygen sensors can severely limit such studies. For example, air–sea oxygen flux depends on the deviation of oxygen concentration from an equilibrium level near 100% saturation (McNeil and D'Asaro 2007). For a typical deviation in oxygen saturation from equilibrium of 1%, a measurement of the flux to an accuracy of 20% requires an absolute accuracy of ~0.2% or ~0.5 μmol kg^{-1} at 15°C. Detection of predicted long-term decreases in oceanic oxygen, typically 0.1 μmol kg^{-1} yr^{-1} (Keeling et al. 2010), place similar tight constraints on sensor accuracy. Manufacturers of the two currently available oxygen sensors quote accuracies an order of magnitude larger. Although previous researchers (e.g., Uchida 2008) report that much higher accuracies can be achieved with careful calibration, uncertainties in calibration and long-term stability remain crucial issues. Here, we address these issues, particularly the long-term stability, with a 4-year-long series of simultaneous *in-situ* calibrations of both sensor types. Although this work was done to calibrate sensors for autonomous float deployments in hurricanes and typhoons, the results have broader applicability.

2. Sensors

a. SBE-43 Clark cell

The SBE-43 oxygen sensor, sold by Seabird Electronics, is a polarographic Clark cell (Carlson 2002; Edwards et al. 2010) that measures the partial pressure of oxygen relative to an internal anoxic standard from the rate of diffusion of oxygen across a membrane separating the sample from the standard. Because this diffusion depletes the oxygen from a thin boundary layer near the membrane, water must be pumped continuously past the membrane to establish an equilibrium. The measurement thus depends on the rate of pumping, which is chosen so that this sensitivity is not large. For applications where power is limited, the pumping rate is reduced, thereby shifting the calibration somewhat. The measurement is also sensitive to physical contamination of the membrane, which changes the rate of diffusion.

The SBE-43 measures the partial pressure (precisely fugacity) of oxygen, or equivalently the oxygen concentration c [μmol kg^{-1}] relative to $c^*(T,S)$ [μmol kg^{-1}], the saturation concentration at standard pressure (1013.25 millibar, 101.324 kPa), a known function of temperature T and salinity S (Garcia and Gordon 1992). Thus the sensor measures $\mathrm{s} = \mathrm{c}/c^*(T,S)$, which we express as a percent. Our sensors output a frequency f proportional to the diffusion rate of oxygen. Other models of the sensor output a voltage with a similar equation. The calibration equation

$$s = F(f)\theta(T)D(P) \tag{1}$$

is the product of three terms. $F(f) = Soc\ (f + F_{offset})$ is a linear function with a gain *Soc*. $\theta(T)$ is quadratic in temperature and describes the temperature response. $D(P) = e^{E\,P/(T+273.15)}$ describes the pressure response. Each sensor is factory calibrated across a matrix of 17 temperature and oxygen values to determine *F(f)* and $\theta(T)$. The function *D* has a minor (0.7%) effect across the range of pressures (0–200 dbar) considered here and Seabird does not change the value of *E*. Residuals from the calibration are typically 0.4 μmol kg^{-1}.

Our SBE-43 sensors were each mounted on the bottom of a Lagrangian float (D'Asaro 2003; Alkire et al. 2012), inline with the pumped Seabird temperature and conductivity sensors. This mounting is upside-down relative to that used in ARGO floats and required that a small hole be drilled in the plumbing to allow air to vent when the float is first submerged. In the measurements described here, the pump was run continuously, but at a slower speed than that used in the factory calibrations. Some of the factory calibrations supplied a correction for this difference (roughly 1–2% in *Soc*). For uniformity, we used the uncorrected values. We evaluated four different sensors (serial numbers 15, 139, 156, 173). The membrane of each sensor was replaced due to damage at some point in the 4-yr evaluation, resulting in seven different sensor/membrane combinations over the period.

b. Aanderaa optode

The 3835 optode sold by Aanderaa Instruments measures the partial pressure of oxygen using the fluorescence quenching (Demas et al. 1999, Klimant et al. 1997) of a

platinum porphyrin complex embedded in a gas permeable foil exposed to the water. Fluorescence is measured using the phase shift φ from an AC modulated blue excitation to the fluoresced red signal. The sensor also measures temperature. It consumes no oxygen and is thus insensitive to the water flow around it.

Under ideal conditions, quenching is described by the Stern–Volmer equation:

$$\mathrm{s} = \left(\frac{\varphi_0}{\varphi} - 1\right)/K\,, \tag{2}$$

where φ_0 is the phase shift at zero oxygen and K is independent of oxygen. Both K and φ_0 are functions of temperature. However, packaging of the fluorescing material and inhomogeneity in its optical properties may lead to more complex forms (Demas et al. 1999). The manufacturer has chosen a calibration equation of the form

$$c = G(c(T), \varphi_d)\, Scorr(T, S)\, Dcorr(P). \tag{3}$$

Oxygen concentration (not partial pressure) is the product of three terms. The function G is a 4th order polynomial in a corrected phase φ_d with coefficients $c(T)$, each of which is a 3rd order polynomial in temperature. *Scorr* expresses the salinity variability of solubility from Garcia and Gordon (1992) and *Dcorr* is a linear pressure correction, again small

over our depth range. The 20 coefficients of G are determined from 35 temperature and oxygen calibration points measured on a sample from a large batch of sensing foil. We have been unable to duplicate the manufacturer's fits from the calibration points. Each foil batch is cut into smaller pieces and used in many different optode sensors. Variability between the foil pieces in each sensor and in the phase calibration of each sensor's electronics is determined from a two-point factory calibration that defines a linear function

$$\varphi_d = a + b\,\varphi_b \tag{4}$$

giving the corrected phase φ_d ('d-phase') from the measured phase φ_b ('b-phase').

We find this calibration scheme inelegant because it ignores the known physical principles on which the sensor operates and uses numerically unstable polynomial forms. For our foils the calibration function [Eq. (3)] has a minimum as a function of φ_b at a value less than 1% below the oxygen zero point and behaves poorly near zero oxygen. When preliminary fits of the form of Eq. (2) to the factory calibration points are compared to the manufacturer's polynomial fits of Eq. (3), the polynomial forms show an increasing deviation from the Stern–Volmer form above 110% saturation, reaching 4% at the last set of calibration points (~135% saturation). Similar large deviations are found at the edges of the calibration domain in all directions. The polynomial forms therefore appear to introduce significant error. However, because this is not the central focus of this paper, we retain the manufacturer's calibrations, but recast them into the form

$$s = \frac{G(c(T), \varphi_d)\, Scorr(T,S)\, Dcorr(P)}{c^*(T,S)} \tag{5}$$

thereby eliminating *Scorr* [because it is part of $c^*(T,S)$] and expressing the calibration in terms of the physical quantity measured.

Our optodes were each also mounted on the bottom of a Lagrangian float, about 12 cm to the side and approximately 20 cm above the intake of the SBE-43 pump [see D'Asaro (2010) for a picture]. We evaluated three sensors (SN 1860,1861, 1862), all with the same batch of foil (SN 1701). The initial factory calibration was used throughout.

3. Calibration methods

a) Approach

Oxygen measurements on autonomous floats have usually not calibrated in detail due to the difficulty of doing this with sufficient accuracy. Calibrations have sometimes been done with casts separated from the float by many days and hours (Kihm and Körtzinger 2010). During NAB08 (Alkire et al., 2012) a single float was calibrated to better than 2 μmol kg^{-1} from 6 Winkler/CTD casts generally within 1 km and 1 hour of the float, a substantial effort. Even with this small separation, many of the Winklers had to be discarded because the shape of the CTD oxygen profiles did not match those measured by

the float. For hurricane deployments, it thus seemed unlikely that we could obtain sufficient accuracy from measurements near the time of deployment. We thus chose to make very accurate *in situ* calibrations in local waters before and after deployment.

b) In situ

Dedicated oxygen calibration efforts were conducted in Puget Sound in July 2008, July 2009, December 2009, July 2010, and December 2010 (Table 1, Fig. 1) to support expected hurricane or typhoon deployments each year. In 2009 and 2010 three or more floats, each with a SBE-43 and optode sensor, were attached to a frame and lowered off the side of the R/V *Robertson* in 100–200 m of water (Fig. 1a). A SBE-9/11 CTD with a 12-bottle, 2-L rosette was lowered a few meters away (Fig. 1b). Both packages were visible in the ship's echosounder (Fig. 1c) and could be navigated to the same depth to within a fraction of one meter. The floats were positioned at several levels chosen to span a wide range of oxygen concentrations and allowed to equilibrate for 2000–3000 s. At each level duplicate bottles were taken at the level of the floats, a few meters above, and a few meters below, for a total of six samples near each level. A single Winkler sample was taken from each bottle. Winkler analyses were done at Seabird Electronics by the same technician and equipment used to calibrate the SBE-43 sensor in Seabird's calibration facility. Differences between the duplicate Winkler samples averaged 0.2 μmol kg^{-1}.

The Winkler data were used to generate a calibration point for each of the floats at each of the levels (Fig. 2). These were interpolated by eye to the float level, guided by the profiles from the CTD. This resulted in a set of calibration points, each with an accuracy of better than 1 μmol kg^{-1}.

Only surface calibrations were used in 2008. Winkler samples were taken within one meter of the sensors using a hand-lowered Niskin bottle from the R/V *Miller*. Winkler samples for float 53 on 21 July were analyzed by C. Stump and were of high quality with a mean difference of duplicates of 0.2 μmol kg^{-1}. Analyses for floats 50 and 51 on 23 July were analyzed by University of Washington Technical Services and had much higher average errors (2 μmol kg^{-1}). Of these, four samples with an average difference in duplicates of 0.5 μmol kg^{-1} were chosen to include in this analysis.

c) Laboratory

Optode calibration points with zero oxygen and some points at 100% saturation were made (Table 2). Zero oxygen calibrations were performed by immersing the float's optode in a saturated sodium sulfite solution. The 100% saturation readings were made with the optode immersed in bubbled water. All readings were made either in a temperature controlled waterbath set at 20°C (when the sensors were detached from the float) or in a large bucket (when the sensors were attached to the float). In both cases, final readings were taken only after the optode's b-phase and internal temperature had fully stabilized. Because the reaction of the sodium sulfite solution with oxygen is exothermic, it can take up to one hour for the readings to stabilize during zero oxygen calibrations.

4. Accuracy and stability of sensors

a) SBE-43

Linear calibrations in oxygen of the SBE-43 sensors to the Winkler calibrations for the July and December tests in Puget Sound typically differ by 3–4% near 100% saturation; the pre-deployment and post-deployment calibrations yield similar results. However, these calibrations span temperatures of 8–13°C and oxygen saturations of 75–110% in summer and 75–100% in winter. Tropical cyclone oxygen values span similar ranges, but with warmer temperatures 22–30°C. Depending on how the differences between the factory and our calibrations are apportioned between temperature and oxygen components of the calibration, different calibrations are obtained. It is thus important to understand which components of the sensor calibration are changing. We analyze 12 SBE-43 factory calibrations for the sensors used on our three floats.

The temperature function $\theta(T)$ varies by 2–3% from 10–30°C (Fig. 3a). Changes in $\theta(T)$ increase with time (Fig. 3b), with a typical rate of 0.3% per year for temperatures near 25°C. For a typical 6-month interval between calibrations, this can account for only ~0.15% change in calibration, much less than was observed. Thus, calibration changes for the SBE-43 sensors are due primarily to changes in the linear frequency function *F(f)*. Variations in the slope of *F(f)*, rather than its offset near zero oxygen, dominate the calibration changes (Fig. 4). We will thus use the limited *in situ* calibration data to vary the slope only.

b. Aanderaa optode

We find large (15%) drifts in the optode, but have insufficient data to assess whether the drift occurs in the temperature [*Scorr* in Eq. (5)] or phase (*G*) components of the calibration. We assume, as for the SBE-43, that all drift is within the phase component.

Figure 5 shows the deviations of the optodes from our calibration points. Although there is insufficient data to define the entire functional form, some features are clear. There is very little (< 1%) change near zero oxygen. The output of the optodes is low compared to the calibrations, with the magnitude of this effect increasing nonlinearly with oxygen and with time. All three optodes behave similarly. The following model captures these features:

$$\delta_s(s_W, t) = s - s_W = \Delta \frac{s_W}{H + s_W} e^{-\frac{t - t_0}{\tau}} \tag{6}$$

where the deviation δ_s of the optode measured oxygen from s_W, the calibration ('Winkler') points, increases with oxygen concentration as described by an amplitude Δ and a half-saturation H, and increases with time t (years) starting from a reference time t_0 with a time scale τ (years). Model parameters are fit to the data by minimizing the sum of the squares of deviation of all points excluding the points near $s \approx 145\%$, a level at which we believe the optode polynomial calibration is inaccurate, and excluding points near $s \approx 0\%$, because the functional form is zero by construction. After fitting, the rms deviation is 0.2%, comparable to the accuracy of the calibration points.

The primary goal of this analysis is to calibrate the optodes near 100% saturation. Accordingly, the model [Eq. (6)] is used to extrapolate the optode reading at each calibration point to 100% saturation, i.e.,

$$s_{100} = s - \delta_s(s_W, t) + \delta_s(100\%, t) \quad (7)$$

equivalent, in Fig. 5, to moving along the constant time line through each data point to $s_W = 100\%$. The resulting time series of optode calibration points at 100% saturation (Fig. 6) show the nearly exponential decrease in the sensitivity of all three optodes, summarized in Eq. (6) by an exponential decay with a time scale of 1.94 years and a total magnitude of 29%. All but 4 of the 69 data points (6%) fall within ±0.7% of this model.

5. Application of calibrations to sensors

The SBE-43 and optode for each float of each deployment were calibrated in three steps. The 2008 calibrations were evaluated at the time of float deployment in Hurricane Gustav; the 2010 calibrations at the deployment time in Typhoon Megi and at a later deployment at Ocean Station Papa. No deployments were made in 2009. The analysis starts with factory calibrated data, which we denote as s_{S0} and s_{O0} for the SBE-43 and optode, respectively.

a) Determine optode offset at 100% saturation and correct optode at 100% saturation

For each float in each deployment, each of the nearest 100% *in situ* calibration points were extrapolated in time to the deployment time using the exponential function in Eq. (6). For example, (Fig. 6 insert) optode 861 (blue) on float 67, deployed in October 2010, was calibrated using four Winkler calibration points from July 2010 and three Winkler points from December 2010. Each was extrapolated in time (thin blue lines) to the deployment time and their mean was taken as the optode offset Δs_O (= –11.8% for

861). The standard error of this estimate was taken as the standard deviation of these points divided by the square root of 7. Floats 66 and 68 (optodes 860 and 862, red and black) have fewer calibration points, but are processed in the same way. An "offset optode" data set s_{O1}, valid at 100% saturation, was computed as $s_{O1} = s_{O0} - \Delta s_O$.

b) Transfer optode calibration to the SBE-43 and correct SBE-43 at all concentration

The SBE-43 and optode were compared at a set of hand-chosen points, excluding times of rapid oxygen change when the slow optode response prevents accurate comparison, and, for some floats, excluding the first few hours of deployment during which the optode does not properly equilibrate. Fig. 7a shows an example for the 2010 deployment of float 67. From its initial deployment to about yearday 289.6 and between yeardays 291.25 and the end of the mission, the float executed a slow vertical profile stopping at selected isopycnals for several hours and producing the stair-like oxygen time series. Between these, the float remained in the mixed layer. Calibration points (yellow) were chosen on each segment of the second profile and in the mixed layer. However, no points were chosen during the first profile when the optode readings were high and noisy.

The offset Δs_S between the offset optode and the factory calibrated SBE-43 at 100% saturation was determined from a linear fit between $s_{S0} - s_{O1}$ and s_{O1} at the comparison points (Fig. 7b), yielding for example, $\Delta s_S = 2.5 \pm 0.4\%$ for float 67. The gain of the SBE-43 was adjusted to match this offset

$$s_{S1} = s_{S0}\,(1 + \Delta s_S/100)^{-1} \tag{8}$$

yielding a calibrated SBE-43 data time series s_{S1} valid at all concentrations. Because the SBE-43 has higher precision and a more certain temperature calibration than the optode, s_{S1} is the primary oxygen data set resulting from this analysis.

c) Recalibrate the optode at all concentrations

The form of the optode calibration shift is not well determined (see section 4b) at saturations different from 100%. A calibrated optode time series, $s_{O2} = A + B\ s_{O1}$, valid over the range of our measurements, was calculated from the linear fit of s_{O1} to s_{s1} at the comparison points. The optode is a secondary data set and the analysis is straightforward so no examples are shown. The calibrated optodes (s_{O2}) deviate by up to ±1% from the calibrated SBE-43 sensors (s_{S1}) at the comparison points.

6. Results

a) Calibrations

Table 3 shows the results of the calibration for each year evaluated at the deployment time for each float. For 2009, with no deployment, the July calibration time was chosen. As expected (Fig. 6), the optode error increased with time. The SBE-43 is -2.3% low on average, comparable to the typical change in sensitivity due to the slower pumping speed in the float than during the factory calibration. The standard deviation around this, about 3.3%, is higher than the manufacturer's specification for initial calibration accuracy, 2%, perhaps reflecting the sum of our calibration uncertainty ~0.4% and some additional drift between the factory calibration and ours. The calibration accuracy is greater for the Ocean Station Papa deployment because the longer records

(~12 days) at nearly 100% saturation make the step described in section 5b more accurate. Floats 66 and 67 were deployed ahead of Typhoon Megi within a few kilometers of each other, yet differed in pre-storm oxygen levels by 0.6%, within the statistical error. Accordingly, they were each shifted by 0.3% so that they agreed.

b) Sanity checks

For Hurricane Gustav, the three calibrated floats measured a pre-storm oxygen level of 100.5–101.5%, within the range of the *2009 World Ocean Atlas* (Garcia et al. 2010) value of 102.5±2%. The deployments were 100 km south of the mouth of the Mississippi River, in a region of potentially strong vertical and horizontal gradients. For Typhoon Megi, the three calibrated floats measured a pre-storm oxygen level of close to 100%. This compares favorably with the *2009 World Ocean Atlas* at the deployment site (100±2%), with the mixed layer oxygen (99.3±0.4%) measured by a SBE-43 on a CTD cast taken 180 km southwest of the float deployment location from the R/V *Revelle*, and with the output of a calibrated optode (99.3±0.95%) plumbed into the seawater system while transiting 200 km west of the float deployment site just before the storm's passage. The shipboard optode was matched to the on-station CTD cast data with an offset of 1.8±0.7% near 100% saturation, and independently checked onboard to have a zero reading of <0.5%.

7. Other sensor issues

The analyses here, and in a comparison of an optode and a SBE-43 mounted on a float during the 2008 North Atlantic Bloom Experiment (NAB08, D'Asaro 2010; Alkire et al. 2012), identified several other issues with both sensors.

During the first day after deployment, the optode data is often noisy and reads high by a few percent (e.g., Fig. 7a). This does not occur at the surface. This might be due to bubbles of air, trapped behind the optical film, which are compressed at depth and diffuse outward through the film.

As has been noted by many others (e.g., Nicholson et al. 2008), the optode's long time response can lead to large hysteresis on profiling instruments. Because the sensor is not pumped, this time can be significantly longer than that specified by the manufacturer (~40 s) depending on how well it is flushed. D'Asaro (2010) reports an optimal value of 153 s on a slowly profiling float, perhaps due to poor flushing around the sensor.

Although the optode does not consume oxygen, biofouling on or near the optode can cause reduced readings in low-flow environments. D'Asaro (2010) reports deviations of up to 13 μmol kg^{-1} compared to a SBE-43 apparently due to this effect. This might also explain the anomalously low oxygen readings measured by Lo Bue (2011) at low current speeds.

The SBE-43 must be pumped to make accurate measurements and thus consumes considerably more energy than the optode (e.g., Martini et al. 2007). One strategy to reduce energy is to pump for long enough to bring the sensor nearly to equilibrium before each sample, typically for 20-40 seconds. However, a complete equilibrium can take much longer than this to achieve [See Edwards (2010) for a detailed analysis of equilibration time.], so that the measured value depends on the oxygen level in the cell

before the pumping starts. When the pumping stops, a new equilibrium oxygen level is established in the cell, with the sensor consuming oxygen and residual flushing restoring it. This equilibrium value and thus the measured oxygen on the next pumping cycle, depends on the local oceanographic conditions. D'Asaro (2010) reports that an SBE-43 operated in this way read up to 3 μmol kg^{-1} high compared to a nearby optode due to the action of surface waves enhancing the sensor flushing near the surface.

In our experience, the optode is more reliable than the SBE-43. All four of the SBE-43 sensors used in our study had their membrane replaced, each once. Only one of the optodes failed.

The SBE-43 appears to have a higher precision, on time scales of 30 s to several hours, than the optode. We have used it to compute vertical oxygen flux by covariance (D'Asaro and McNeil 2007). Similar attempts using optodes mounted on the same floats have yielded only noise.

8. Summary and discussion

The major surprise in this study was the long-term (multiyear) predictable drift of the optodes during storage, which runs contrary to other reports (e.g., Tengberg et al. 2006) of high stability. Aanderaa (personal communication, 2012) reports drifts of similar magnitudes attributed to photobleaching of the optode by the sensor's blue LED during the first ~10^5 samples and now 'burns-in' new optodes to limit this effect. Our sensors were not 'burned in', but their drift does not appear to be related to sampling. The observed drift was remarkably stable and nearly independent of the details of how

the optodes were stored and/or operated, which varied between sensors in different years. In most years, between deployments the optodes remained attached to the bottom of the floats; the floats were stored in the corner of a windowless basement room with fluorescent lights that were mostly on during working days. Typically, they were shipped by truck to Keesler Air Force Base in Mississippi in early August inside of wooden shipping boxes cushioned by closed cell foam. These boxes were stored in an aircraft hanger until deployment in late August or early September. After a few weeks in the ocean, they were recovered, any biofouling removed, put back in boxes and shipped to Seattle. In some years, the optodes were coated with glycerin. In particular, between the calibrations in July and December 2009, the optodes were not run at all and remained at Keesler in boxes through October. Nevertheless, the same amount of drift was observed. We speculate that the drift may be due to some environmental factor during storage, for example atmospheric ozone, but cannot identify it. It is possible that the observed decay does not occur for optodes in the ocean, due perhaps to the absence of this factor.

The factory calibrations of both sensors were insufficient to obtain accuracies in excess of 1%, as needed for most estimates of air–sea gas transfer. Because the errors of the two different sensors are different, combining both types on the same platform led to a more robust measurement and allowed diagnosis of errors in both. This, combined with repeated, high-accuracy, *in-situ* calibrations were the key elements allowing the required accuracies and precisions to be obtained, both here and during NAB08 (D'Asaro 2010; Alkire et al. 2012).

Accurate interpretation of limited calibrations requires calibration equations that match well the physics of the sensors. Because both sensors measure partial pressure, or

equivalently percent saturation at standard pressure, it is best to analyze calibration data for these sensors in terms of this quantity. Our analyses provide additional guidance: Drift of the SBE-43 occurs primarily in the sensor gain [*Soc* in Eq. (1)]; the zero point (*Foff* Soc*) and the temperature compensation [$\theta(T)$] are more stable. Drift in the optode is highly predictable and is much larger at 100% saturation than in anoxic conditions. The environmental factors causing this drift are unknown; its complete functional form is also unknown, but is nonlinear in oxygen and a decaying exponential in time. We anticipate that using a Stern–Volmer form [Eq. (2)] to calibrate the optode rather than a polynomial would lead to more insight and plan to reanalyze these data using this approach.

Acknowledgments

This work was supported by the National Science Foundation under grants OCE 0549887 and 0834340 and benefitted from logistics supplied as part of the Office of Naval Research ITOP program. Floats were air-deployed by the 53rd Weather Reconnaissance Squadron, Air Force Reserve Command, 'Hurricane Hunters'. The engineers and staff of the Applied Physics Laboratory provided essential support as did the officers and crew of the R/V *Revelle*, R/V *Cape Hatteras*, and R/V *Robertson*.

References

Alkire, M.B., E.D'Asaro, C. Lee, M. J. Perry, A. Gray, I. Cetinić, N. Briggs, E. Rehm, E. Kallin, J. Kaiser, and A. González-Posada, 2012: Estimates of net community production and export using high-resolution, Lagrangian measurements of O_2, NO_{3-}, and POC through the evolution of a spring diatom bloom in the North Atlantic. *Deep Sea Res. I*, **64**, 157–174, doi:10.1016/j.dsr.2012.01.012.

Carlson, J., 2002: Development of an optimized dissolved oxygen sensor for oceanographic profiling. *Int. Ocean Sys*., **6**, 20–22.

D'Asaro, E.A., 2003: Performance of autonomous Lagrangian floats. *J. Atmos. Ocean. Technol.*, **20**, 896–911, doi:10.1175/1520-0426(2003)020<0896:POALF>2.0.CO;2

D'Asaro, E., and C. McNeil, 2007: Air–sea gas exchange at extreme wind speeds measured by autonomous oceanographic floats. *J. Marine Sys.*, **66**, 92–109.

D'Asaro, E., 2010: Calibration of the dissolved oxygen sensors on float 48 and on the *Knorr* CTD with Winkler bottle samples, *The 2008 North Atlantic Bloom Experiment, Calibration Report #3*. Archived at the Biological and Chemical Oceanography Data Management Office, http://data.bco-dmo.org/NAB08/Oxygen_Calibration-NAB08.pdf

Demas, J.N, B.A. DeGraff, and P. Coleman, 1999: Oxygen sensors based on luminescence quenching, *Anal. Chem.,* **71**, 793A-800A.

Edwards, B., D. Murphy, C. Janzen, and N. Larson, 2010: Calibration, response, and hysteresis in deep-sea dissolved oxygen measurements. *J. Atmos. Ocean. Technol.*,

27, 920–931, doi:10.1175/2009JTECHO693.1.

Garcia, H.E., and L.I. Gordon, 1992: Oxygen solubility in seawater: Better fitting equations. *Limnol. Oceanogr.*, **37**, 1307–1312.

Garcia, H.E., R.A. Locarnini, T.P. Boyer, J.I. Antonov, O.K. Baranova, M.M. Zweng, and D.R. Johnson, 2010: *World Ocean Atlas 2009, Volume 3: Dissolved Oxygen, Apparent Oxygen Utilization, and Oxygen Saturation*. S. Levitus, Ed. NOAA Atlas NESDIS 70, U.S. Government Printing Office, Washington, D.C., 344 pp.

Keeling, R., A. Kortzinger, and N. Gruber, 2010: Ocean deoxygenation in a warming world. *Annu. Rev. Mar. Sci.,* **2**, 199–229, doi:10.1146/annurev.marine.010908.163855.

Kihm, C., and A. Körtzinger, 2010: Air–sea gas transfer velocity for oxygen derived from float data. *J. Geophys. Res.*, **115**, C12003, doi:10.1029/2009JC006077.

Klimant et al., 1997, Optical measurement of oxygen and temperature in microscale: strategies and biological applications. Sensors and Actuators B 38-39, 29-37, 1997.

Körtzinger, A., J. Schimanski, and U. Send, 2005: High quality oxygen measurements from profiling floats: A promising new technique. *J. Atmos. Ocean. Technol.*, **22**, 302–308. doi:10.1175/JTECH1701.1.

Lo Bue, N., A. Vangriesheim, A. Khripounoff, and T. Soltwedel, 2011: Anomalies of oxygen measurements performed with Aanderaa optodes. *J. Operation. Oceanogr.*, **4**, 29–39.

Martini M., B. Butman, and M. Mickelson, 2007: Long-term performance of Aanderaa

optodes and Sea-Bird SBE-43 dissolved-oxygen sensors bottom mounted at 32 m in Massachusetts Bay. *J. Atmos. Ocean. Technol.*, **24**, 1924–1935.

McNeil, C., and E. D'Asaro, 2007: Parameterization of air–sea gas fluxes at extreme wind speeds, *J. Marine Sys.*, **66**, 110–121.

Nicholson, D., S. Emerson, and C. Erickson, 2008: Sub mixed-layer oxygen production determined from Seaglider surveys. *Limnol. Oceanogr.,* **53**:2,226–2,236.

Prakash S., T.M. Balakrishnan Nair, T.V.S. Udaya Bhaskar, P. Prakash, and D. Gilbert, 2012: Oxycline variability in the central Arabian Sea: An Argo-oxygen study, *J. Sea Res.,* **71**, 1–8, doi:10.1016/j.seares.2012.03.003.

Riser, S., and K. Johnson, 2008: Net production of oxygen in the subtropical ocean. *Nature*, **451**, 323-325.

Tengberg, A., J. Hovdenes, H.J. Andersson, O. Brocandel, R. Diaz, D. Hebert, T. Arnerich, C. Huber, A. Körtzinger, A. Khripounoff, F. Rey, C. Rönning, J. Schimanski, S. Sommer, and A. Stangelmayer, 2006: Evaluation of a lifetime-based optode to measure oxygen in aquatic systems. *Limnol. Oceanogr. Methods*, **4**, 7–17.

Uchida, H., T. Kawano, I. Kaneko, and M. Fukasawa, 2008: In situ calibration of optode-based oxygen sensors. *J. Atmos. Ocean. Technol.*, **25**, 2271–2281, doi:10.1175/2008JTECHO549.1

Table 1. Puget Sound Calibrations

Dates	Float	Optode/Foil	SBE43	Method	Field Deployments
Jul 21–23	50	860 /1707	015	1,a,b	Before Hurricane Gustav
2008	52	861 /1707	120		~3 day operation
	53	862 /1707	152		~18 days in water
Jul 9, 13	54	860 /1707	152	2,c	Pre- and post 2009
Dec 1	55	861 /1707	015		No hurricane deployments
2009	56	862 /1707	139		
Jul 7, 9	66	860 /1707	173	2,c	Before and After Typhoon Megi
Dec 13	67	861 /1707	015		~3 day operation
2010	68	862 /1707	139		~6 days in water
	63	861/1707	156		Before PAPA deployment 862

Water sampling by
1. Lowered Niskin bottle
2. CTD rosette

Winkler Analysis
a. UW technical services
b. C. Stump
c. Seabird Electronics

Table 2. Optode Laboratory Calibrations

Optode SN	Apr 2008	Jul 2008	Oct 2008	Aug 2012
860	Z, S	Z	Z	Z, S
861	Z, S	Z	Z	Z, S
862	Z, S	Z	Z	Z

Z=zero, S=100% saturation

Table 3. Calibration Results

Float	Time	Storm	Optode	Offset[1,2]	SBE-43	Offset[1,3]
50	Sep 2008[a]	H. Gustav	860	–4.8±0.2	15	–1.2±0.4
52	Sep 2008[a]	failed	861	–4.9±0.2	120	—
53	Sep 2008 [a]	H. Gustav	862	–3.8±0.04	152	–3.2±0.3
54	Oct 2009[b]	—	860	–8.5±0.3	152	–5.8±0.4
55	Oct 2009[b]	—	861	–9.0±0.1	15	–3.6±0.4
56	Oct 2009[b]	—	862	–8.8±0.1	139	–4.1±0.4
66	Oct 2010[a]	T. Megi	860	–11.8±0.07	173	3.4±0.3
67	Oct 2010[a]	T. Megi	861	–12.2±0.2	15	2.5±0.4
68	Oct 2010[a]	T. Megi	862	–12.1±0.1	139	–6.3±0.5
63	Feb 2011[a]	Ocean Station Papa	861	–12.6±0.1	156	–2.8±0.1
					Bias[4]	–2.3±1.1
					Accuracy[5]	0.4

a. At time of float deployment in storm. b. At July 2009 calibration.
1. Offset (%) of factory calibration from interpolated Winkler samples at 100% saturation at 1013.25 mbar. Errors are 2 standard deviations.
2. Valid only at 100% saturation. Calibration at other levels is not well known.
3. Calibration at other oxygen levels is factory calibration times $(1 + \mathrm{Offset}/100)^{-1}$.
4. Mean of all SBE-43 offsets ± 2 standard deviations of mean.
5. Mean of SBE-43 offset uncertainties excluding Ocean Station Papa.

Figures

Fig. 1. Puget Sound calibrations of multiple floats. a) A rack holding five floats was lowered over the port side by the research vessel's crane. b) A SBE-9/11 CTD with rosette was deployed off the fantail and took water samples close to the operating floats. c) The two packages could be navigated in the vertical to a fraction of one meter using the vessel's echosounder and were no more than 10 m apart horizontally.

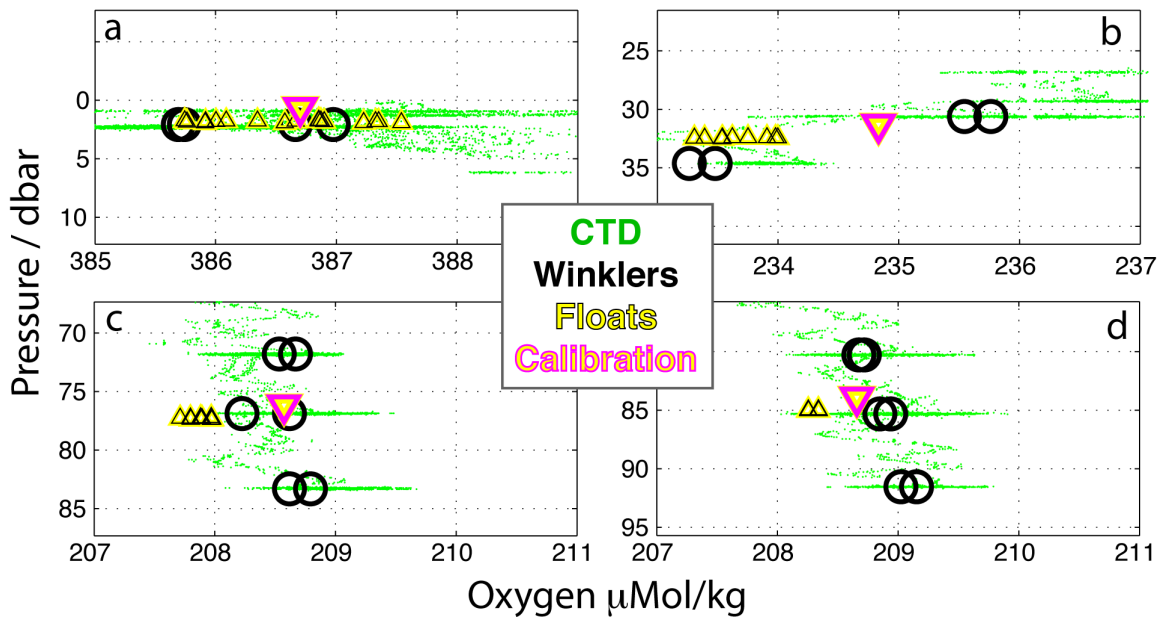

Fig. 2. Determination of four of the five calibration points for July 2010. Duplicate Winkler samples at each level (black circles) were taken at, above, and below the float package (small yellow triangles) guided by data from the CTD (green dots). A calibration point (magenta triangle) for the floats based on the Winkler samples was chosen at each level. Accuracies of better than 1 μmol kg^{-1} were achieved. The float and CTD oxygen values have been offset from their factory calibrations in this figure to best show their relative variations.

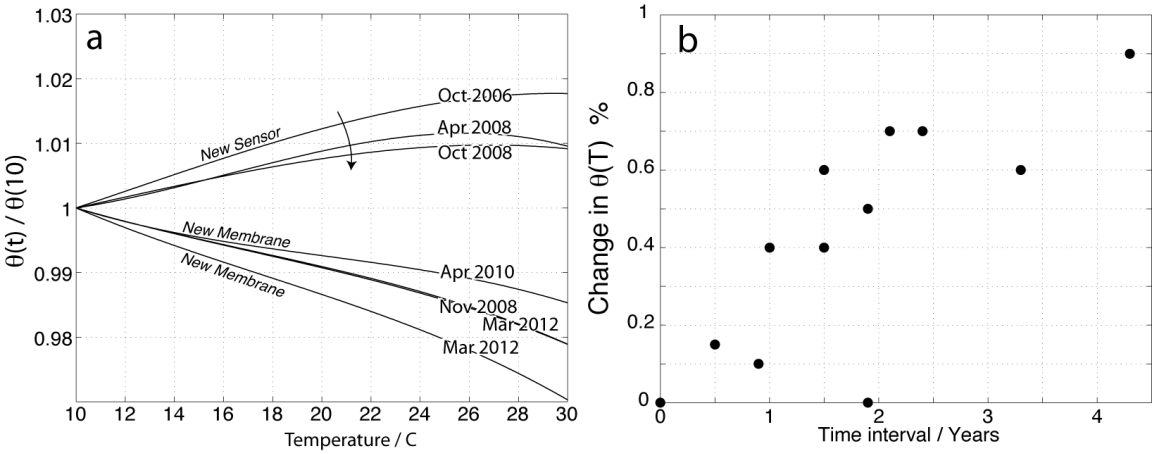

Fig. 3. Variations in the SBE-43 temperature function. a) $\theta(T)$ for six different calibrations of sensor #15 normalized by the value at T=10°C and labeled by date. The membrane was changed between the 3rd and 4th calibrations and for the last calibration. b) Absolute value of change in $\theta(T)/\theta(10)$ near 25°C as a function of time interval between calibrations for all sensors.

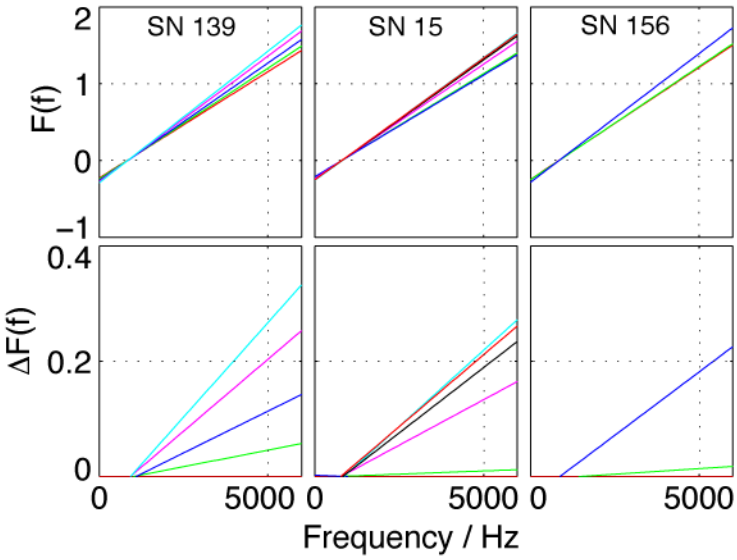

Fig. 4. *Top row:* The SBE-43 frequency function *F(f)* for sensors 139, 15, and 156 at multiple calibrations each with a different color. *Bottom row:* Deviation of *F*(*f*) from the first calibration.

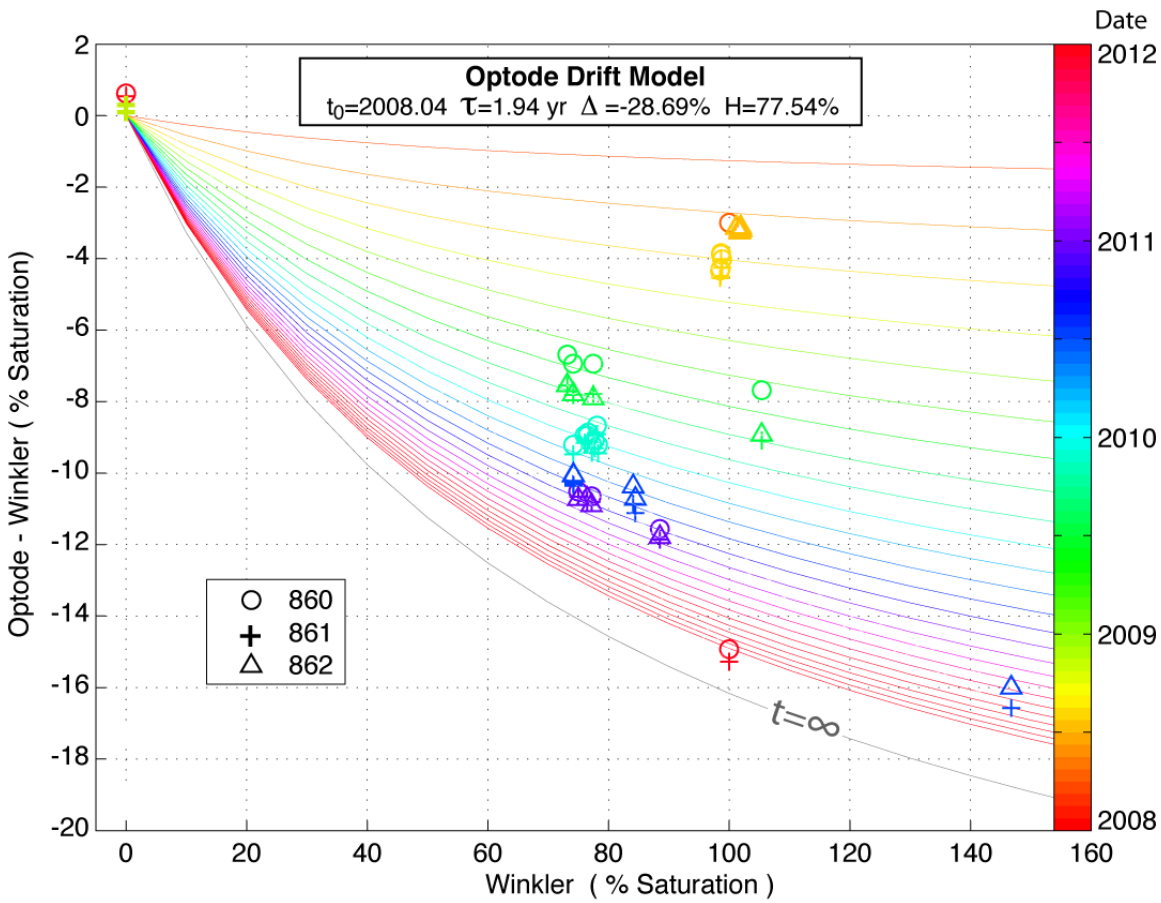

Fig. 5. Deviation of optode oxygen from *in situ* and laboratory calibrations for three optodes all with the same batch of membrane. Optode oxygen was calculated using the factory calibration. Color indicates time; symbol type indicates optode number. Lines, also colored by time, show a model [Eq. (6)] that approximately fits these data.

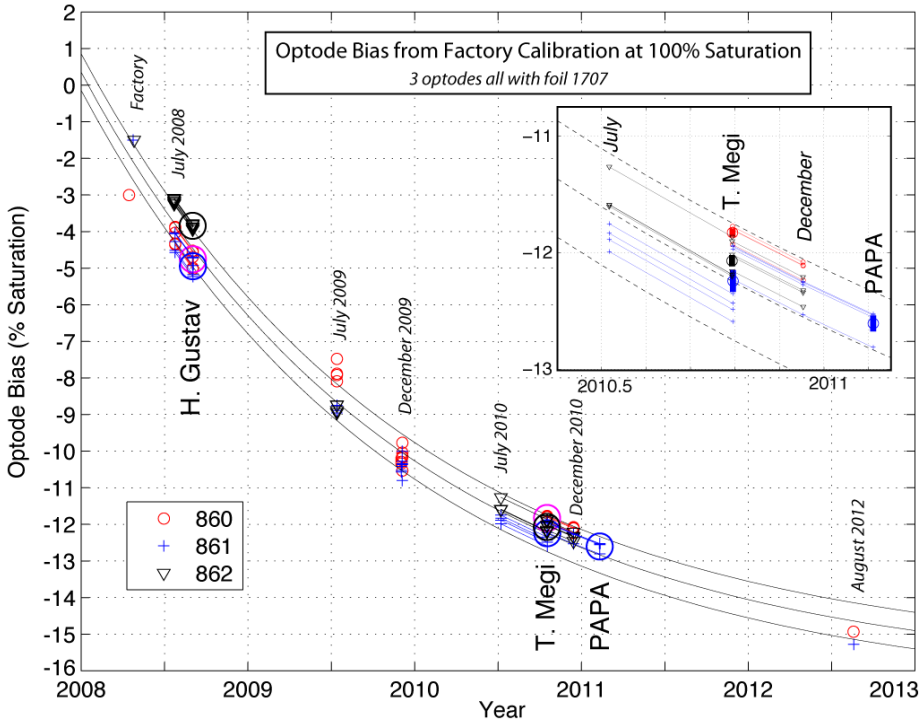

Fig. 6. Optode bias at 100% saturation as a function of time. Small symbols and text show individual calibration points. Large symbols and text show these points interpolated to float deployment times. Gray lines show optode model [Eq. (6)] with a spread of ±0.5%. Insert shows details of interpolation for Typhoon Megi and Ocean Station PAPA deployments with heavy bars spanning the calibration value ± its estimated standard deviation. Colors and symbol type distinguish the three different optodes.

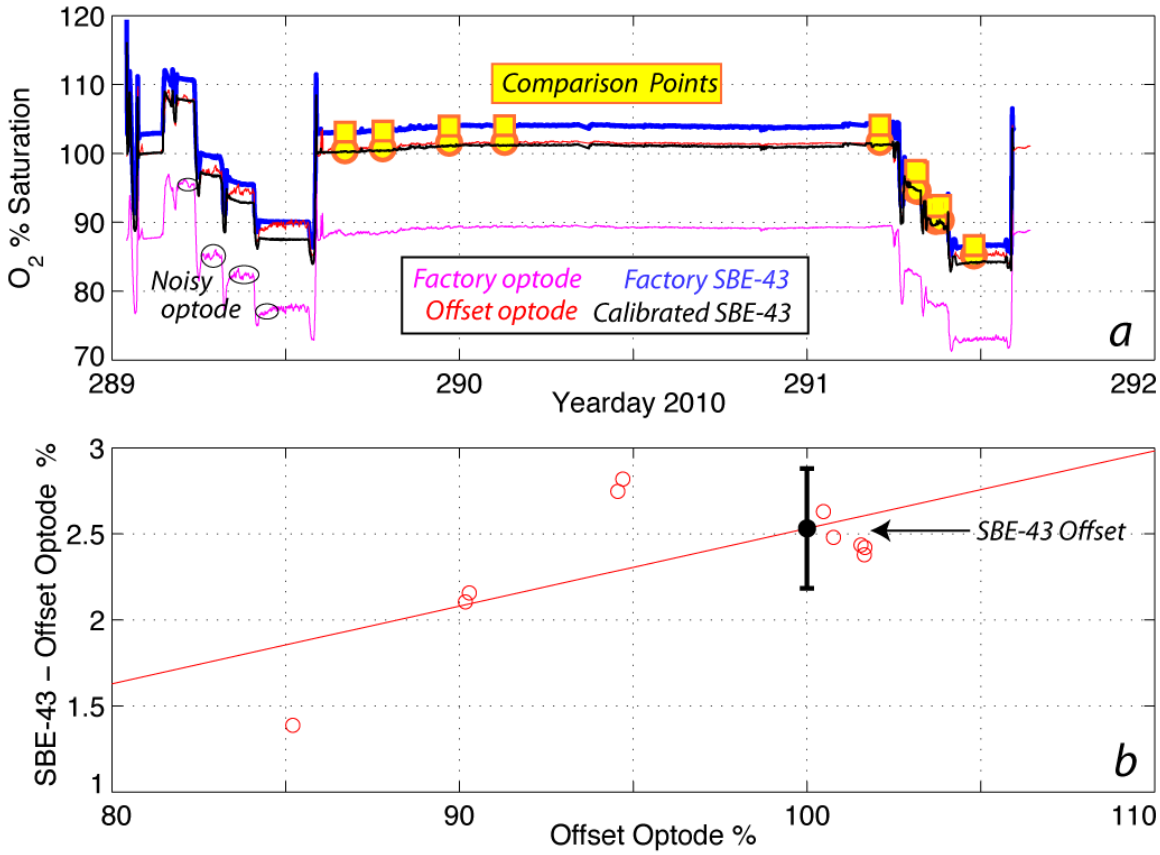

Fig. 7. a) Time series of oxygen for float 67, optode 861, measured during Typhoon Megi marked with comparison points (yellow). Factory calibrated optode (magenta) is offset (red) based on extrapolated Winkler samples. Factory calibrated SBE-43 (blue) is scaled based on optode offset to form the final SBE-43 calibrated data (black). b) A least squares fit between the SBE-43 – optode difference and the oxygen level at the comparison points gives the SBE-43 offset at 100% saturation.